British Journal of Pharmacology

DOI:10.1111/bph.13279
www.brjpharmacol.org

RESEARCH PAPER

High glucose-induced changes in hyaloid-retinal vessels during early ocular development of zebrafish: a short-term animal model of diabetic retinopathy

Seung-Hyun Jung †, Young Sook Kim †, Yu-Ri Lee and Jin Sook Kim

Korean Medicine Convergence Research Division, Korea Institute of Oriental Medicine (KIOM), Daejeon 305-811, Korea

Correspondence
Jin Sook Kim, Korean Medicine Convergence Research Division, Korea Institute of Oriental Medicine (KIOM), 1672 Yuseongdae-ro, Yuseong-gu, Daejeon 305-811, Korea.
E-mail: jskim@kiom.re.kr
†These authors contributed equally to this work.

Received
2 April 2015
Revised
6 August 2015
Accepted
7 August 2015

BACKGROUND AND PURPOSE

Although a variety of animal models have been used to test drug candidates and examine the pathogenesis of diabetic retinopathy, time-saving and inexpensive models are still needed to evaluate the increasing number of therapeutic approaches.

EXPERIMENTAL APPROACH

We developed a model for diabetic retinopathy using the early stage of transgenic zebrafish (*flk*:EGFP) by treating embryos with 130 mM glucose, from 3-6 days post fertilisation (high-glucose model). On day 6, lenses from zebrafish larvae were isolated and treated with 3% trypsin, and changes in hyaloid-retinal vessels were analysed using fluorescent stereomicroscopy. In addition, expression of tight junction proteins (such as zonula occludens-1), effects of hyperosmolar solutions and of hypoxia, and *Vegf* expression were assessed by RT –PCR. NO production was assessed with a fluorescent substrate. Effects of inhibitors of the VEGF receptor, NO synthesis and a VEGF antibody (ranibizumab) were also measured.

KEY RESULTS

In this high-glucose model, dilation of hyaloid-retinal vessels, on day 6, was accompanied by morphological lesions with disruption of tight junction proteins, overproduction of *Vegf* mRNA and increased NO production. Treatment of this high-glucose model with an inhibitor of VEGF receptor tyrosine kinase or an inhibitor of NO synthase or ranibizumab decreased dilation of hyaloid-retinal vessels.

CONCLUSIONS AND IMPLICATIONS

These findings suggest that short-term exposure of zebrafish larvae to high-glucose conditions could be used for screening and drug discovery for diabetic retinopathy and particularly for disorders of retinal vessels related to disruption of tight junction proteins and excessive VEGF and NO production.

Abbreviations

DA, dorsal aorta; dpf, day post-fertilization; DR, diabetic retinopathy; HG, high glucose; ISVs, intersomitic vessels; OD, optic disc; ZO-1, zonula occludens-1

Tables of Links

TARGETS
Catalytic receptors[a]
VEGFR, VEGF receptor
Enzymes[b]
NOS

LIGANDS
L-NAME
NO
Ranibizumab
VEGF

These Tables list key protein targets and ligands in this article which are hyperlinked to corresponding entries in http://www.guidetopharmacology.org, the common portal for data from the IUPHAR/BPS Guide to PHARMACOLOGY (Pawson *et al.*, 2014) and are permanently archived in the Concise Guide to PHARMACOLOGY 2013/14 ([a b] Alexander *et al.*, 2013a,b).

Introduction

Hyperglycaemia is involved in retinal vascular dysfunction associated with the development of diabetic retinopathy (DR), which results in worsening vision and eventual blindness. Nearly all patients with type 1 and type 2 diabetes exhibit some lesions after 20 years with disease (Kempen *et al.*, 2004; Roy *et al.*, 2004; Calcutt *et al.*, 2009). As early DR progresses, non-proliferative DR enters an advanced proliferative stage. Loss of pericytes, retinal vasculature thickening and disruption of tight junction proteins such as zonula occludens-1 (ZO-1) are found in the early stages of DR (Checchin *et al.*, 2006; Pfister *et al.*, 2008). Furthermore, these events result in decreased circulation, blood vessel dilation and obstruction, and increased leakage of blood from the microvascular circulation, thereby increasing VEGF signalling. Increased VEGF signalling causes the formation of new blood vessels from retinal tissues (Guillemin and Brew, 2004; Armulik *et al.*, 2005; Bergers and Song, 2005; Checchin *et al.*, 2006; Alvarez *et al.*, 2010). These vascular changes, collectively, cause a breakdown of the blood-retinal barrier and compromise retinal function. Neovascularization on the retina and posterior surface of the vitreous, and macular oedema characterized by retinal thickening from leaky blood vessels, develop during various stages of retinopathy (Fong *et al.*, 2003). Moreover, expression of endothelial NOS (eNOS), a downstream mediator of VEGF activity, was increased in diabetic retina, and eNOS inhibition also potently reduced retinal leukocyte adhesion (Joussen *et al.*, 2002). Several studies indicate that NO plays a crucial role in VEGF-induced vascular hyperpermeability and angiogenesis (Morbidelli *et al.*, 1996; Lakshminarayanan *et al.*, 2000). Additionally, VEGF induces the expression of NOS and stimulates production of NO (Abu El-Asrar *et al.*, 2004). Therapeutic approaches such as VEGF inhibitors, aldose reductase inhibitors, NOS inhibitors, antioxidants, anti-inflammatory agents and the receptor for advanced glycation end products are proposed interventions for treating DR (Greene *et al.*, 1999; Joussen *et al.*, 2002; Starita *et al.*, 2007; Calcutt *et al.*, 2009).

Many species, including dogs, hamsters, rats, mice and zebrafish, have been used to provide research models for DR (Engerman and Kern, 1995; Jorgens *et al.*, 2012). These models employ chemical or genetic modifications to induce early stages of DR, including degeneration of retinal capillaries (Kempen *et al.*, 2004). Zebrafish are an attractive animal model for molecular, toxicological and drug development studies because of their fecundity, as well as their genetic and physiological similarities to mammals (Barros *et al.*, 2008). They are generally suited to high-throughput screening because of their small size, high productivity and optical transparency of the embryo (Kitambi *et al.*, 2009). Furthermore, techniques for generating transgenic lines and gene-targeting mutations have been developed for zebrafish, enabling the establishment of disease models for drug discovery. The immersion of adult or larvae zebrafish in glucose (0.7–25%) results in diabetic complications, which share similarities with streptozotocin (STZ)-induced diabetic mice and diabetic patients (Gleeson *et al.*, 2007; Alvarez *et al.*, 2010; Liang *et al.*, 2010; Jorgens *et al.*, 2012). Additionally, in retinas of adult zebrafish exposed for 30 days to hyperglycaemia, there are morphological changes such as thickening of the vessels, breakdown of interendothelial cell–cell junction integrity and vessel basement membrane thickening (Gleeson *et al.*, 2007; Alvarez *et al.*, 2010). In larval zebrafish, anti-diabetic compounds reduce expression of phosphoenolpyruvate carboxykinase, which catalyses a rate-limiting step in gluconeogenesis and is transcriptionally regulated by glucagon and insulin. Data have shown that larvae zebrafish are an appropriate model for the study of glucose metabolism (Elo *et al.*, 2007). Our previous study, we tested the inhibitory effect of single compounds isolated from herbal extracts on hyaloid-retinal vessel dilation in glucose-induced larval zebrafish (Lee *et al.*, 2013; Yu *et al.*, 2013). However, changes of tight junctions in retinal vessels in glucose-induced zebrafish larvae have not previously been described in a short-term model for selection of effective agents against DR.

Here, to examine the potential of larval zebrafish as a model for DR, we exposed zebrafish embryos, from *flk*:EGFP transgenic fish, to a range of concentrations of glucose for 3 days, and isolated the retina. Alterations in thickness of the hyaloid-retinal vessels, expression of the tight junction protein ZO-1, vascular leakage and mRNA expression for *Vegf* and *nos* were measured in glucose-exposed zebrafish larvae. We also tested the effects of an inhibitor of VEGFR tyrosine kinase, an inhibitor of NOS (L-NAME) and the clinically used VEGF antibody ranibizumab (FDA approved drug for DR).

Methods

Zebrafish maintenance

All animal husbandry and experimental protocols complied with institutional guidelines and were approved by local ethical boards (Korea Institute of Oriental Medicine Animal Care and Use Committee). Studies involving animals are reported in accordance with

the ARRIVE guidelines for reporting experiments involving animals (Kilkenny *et al.*, 2010; McGrath *et al.*, 2010). Adult zebrafish were maintained under standard conditions at 28.5°C with a 14 h light/10 h dark cycle (Nusslein and Dahm, 2002). Embryos were obtained from crosses between *flk*:EGFP transgenic fish and raised in embryonic water. Transgenic zebrafish (*flk*:EGFP) were provided by Professor C-H. Kim (Chungnam National University). Embryonic stages were determined by days post-fertilization (dpf). Fluorescent images were collected at 6 dpf using a fluorescent dissecting microscope SZX16 (Olympus, Tokyo, Japan).

Treatments and measurement of glucose levels

Zebrafish transgenic (*flk*:EGFP) embryos (3 dpf) were placed in 24-well plates (five embryos per well) and maintained in 2 mL embryonic water (sea salt, Sigma, USA, 0.06 $g \cdot L^{-1}$) containing a range of concentrations of glucose (30, 60, 90, 120, 125, 130, 135 and 150 mM). Media were maintained for 3 days, and embryos were fixed, and survival rates were analysed at 6 dpf. In later experiments, embryos were exposed to a single concentration of glucose (130mM) from 3 to 6 dpf and are referred to as high glucose (HG)-treated larvae.

To assess the effects of hyperosmolarity, embryos were exposed to mannitol (130 mM; Sigma, USA, Cat. No. C8661), instead of glucose, but under the same conditions. To assess effects of hypoxia, embryos were exposed to $CoCl_2$ (120 μM; Sigma, USA, Cat. No. M9546) instead of glucose, but under the same conditions. The effects of the VEGF receptor tyrosine kinase inhibitor (0.5 or 1 μM; Calbiochem, Germany, Cat. No. 676500), or ranibizumab (1 or 2.5 $\mu g \cdot mL^{-1}$; Lucentis, Novatris, Stein, Switzerland) or L-NAME (10 or 20 μM; Sigma, USA, Cat. No. N5751) were tested by addition to the HG treatment for 3 days.

Quantitative analysis of glucose levels was performed from whole body lysates using a glucose assay kit (Sigma, USA). Briefly, 20 zebrafish larvae in each experimental group were sonicated in 500 μL deionized water on ice. According to the instructions, standard curves were generated using glucose standard solution. A total of 2 mL assay reagent (Sigma) was added and incubated for 30 min at 37°C. Fluorescence (540 nm) was measured using a BioTek plate reader equipped with GEN5 software (v.2.04, BioTek, Winooski, VT, USA).

Lens isolation and measurement of hyaloid-retinal vessel diameter

At 6 dpf, zebrafish larvae were fixed with 4% paraformaldehyde and stored overnight at 4°C. They were then washed with distilled water (1.5 ml per well, 3 times within 1 h) and lenses containing hyaloid-retinal vessels were isolated after incubation with 3% trypsin in Tris–HCl buffer (pH 7.8), for 80 min at 37°C (Figure 1). Images of hyaloid-retinal vessels, optic disc (OD) branches and lens size were obtained using an Olympus stereomicroscope (SZX16) or a laser scanning confocal microscope (FV10i, Olympus, Tokyo, Japan). Their diameters were determined by IMAGEJ software (Figure S1).

Total RNA extraction and RT-PCR

Total RNA from whole embryos was extracted using TRIzol reagent according to the manufacturer's protocol (iNtRON, Korea) and reverse transcribed using M-MLV reverse transcriptase (Invitrogen, USA). The reverse transcription (RT) product (1 μL) was used as a template for PCR amplification of *Vegf*165 and β-*actin* using specific primers (5 pM; Genotech, Korea), Taq DNA polymerase (Elpis, Korea) and the following cycles: 95°C for 30 s, 55°C for 30 s and 68°C for 40 s for 30 cycles. Primer pairs were as follows: *Vegf*165, forward primer 5′-CTC CTC CAT CTG TCT GCT GTA AAG-3′ and reverse primer 5′-CTC TCT GAG CAA GGC TCA CAG-3′; *nos2a*, forward primer 5′-GTG TTC CCT CAG AGA ACA GAT-3′ and reverse primer 5′-GAT CAG TCC TTT GAA GCT GAC-3′; and β-*actin*, forward primer 5′-GAG AAG ATC TGG CAT CAC AC-3′ and reverse primer 5′-ATC AGG TAG TCT GTC AGG TC-3′. PCR products were separated by electrophoresis on 1.2% agarose gels and visualized by ethidium bromide staining.

Whole-mount immunostaining

Whole-mount immunostaining was performed as previously described (Jung *et al.*, 2010) using primary antibodies against mouse ZO-1 (1:500, Invitrogen, USA). For fluorescent detection of antibody labelling, we used Alexa Fluor 568 anti-mouse conjugate (1:500, Molecular Probes, Eugene, OR, USA) and Hoechst 33342 (1:1000, Thermo Fisher Scientific, Waltham, MA, USA). Fluorescence images were examined using an Olympus laser scanning confocal microscope (FV10i).

NO detection

Live imaging detection of NO production was carried out as described by Lepiller *et al.* (2007). Briefly, wild-type larvae treated with control and HG at 6 dpf were incubated in 5 μM 4,5-diamino-fluorescein diacetate (DAF-FM DA) (Molecular Probes) for 30 min, rinsed in egg water, anaesthetized and imaged using Olympus laser scanning confocal microscopy (FV10i).

Data analysis

Results are expressed as the mean ± SEM of multiple experiments. Experimental data are from 40–60 embryos per treatment, from 2–3 independent clutches. Data were analysed using one-way ANOVA with Tukey's *post hoc* analysis or unpaired Student's *t*-tests and PRISM software (GraphPad, San Diego, CA, USA). $P < 0.05$ was considered statistically significant.

Results

Glucose-induced changes in hyaloid-retinal vessels in zebrafish larvae

Because chronic hyperglycaemia is a feature of human type 2 diabetes, we hypothesized that adequate exposure to HG conditions would induce metabolic disturbances that are similar to DR models. Thus, retinal vascular changes in HG zebrafish may reflect similar changes observed in mammalian models. To investigate changes in hyaloid-retinal vessels induced by HG in zebrafish Tg (*flk*:EGFP), we exposed embryos to an range of concentrations of glucose (30–150 mM) from 3 to 6 dpf and analysed the diameter of the hyaloid-retinal vessels obtained at 6dpf (Figure 2). The hyaloid-retinal vasculature begins to be generated on 2.5 dpf in normal zebrafish development (Alvarez *et al.*, 2007). Thus, we exposed embryos for 3 days, from 3 to 6 dpf to the different levels of glucose. The experimental protocols used to measure glucose-induced changes in hyaloid-retinal vessel diameter in zebrafish embryos are summarised in Figure 1 (and S1). Using retinae isolated at 6 dpf, we found that

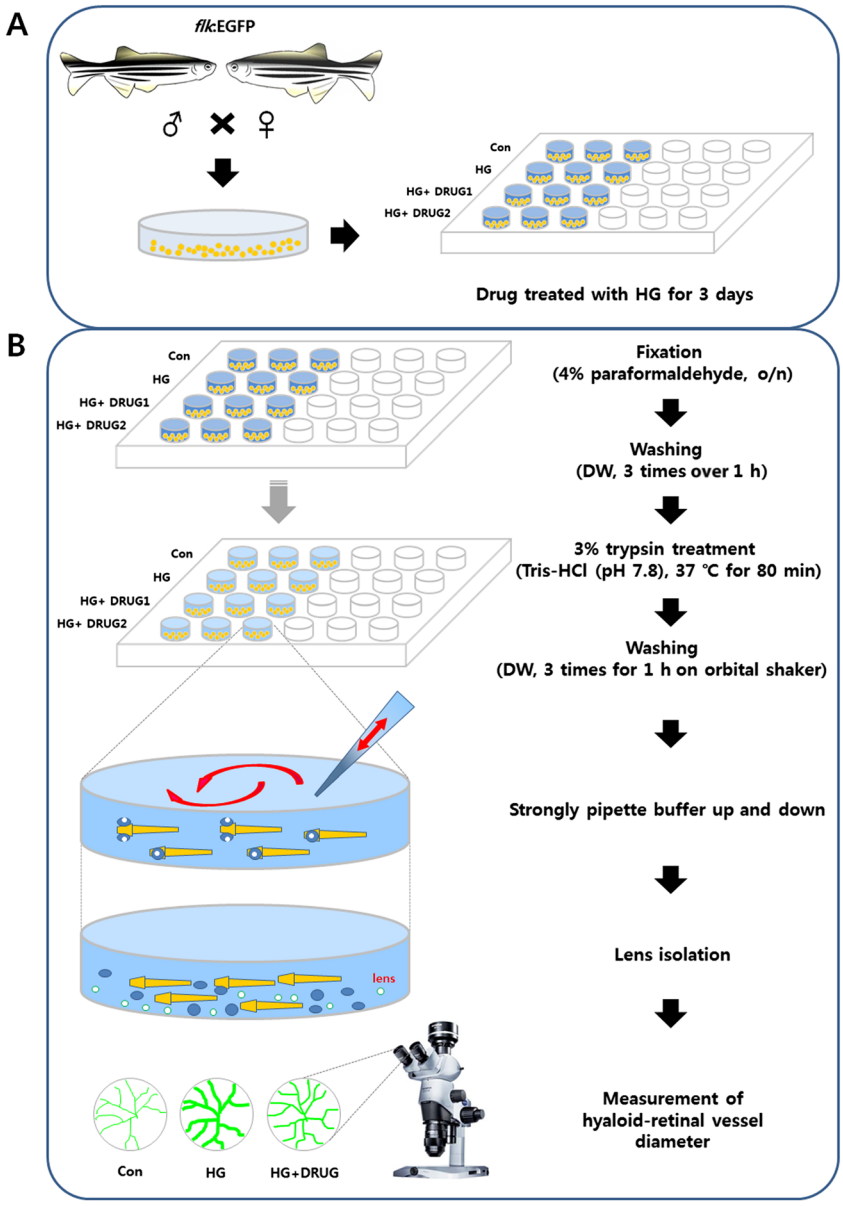

Figure 1

Overall strategy for rapid screening to identify therapeutic drugs for DR in zebrafish larvae. (A) Fertilized embryos from zebrafish Tg (*flk*:EGFP) pairs were produced. GFP-positive embryos at 3 dpf were placed in 24-well plates and maintained in embryonic water containing high concentrations of glucose (130 mM; HG) and candidate drugs. (B) At 6 dpf, larvae deposited in 24-well plates were fixed with 4% paraformaldehyde and stored overnight at 4°C. After washing three times for 1 h with distilled water (DW), larvae were incubated for 80 min with 3% trypsin [Tris–HCl (pH 7.8)] at 37°C and washed three times for 1 h with DW on an orbital shaker at room temperature. Using a stereomicroscope, lenses with hyaloid-retinal vessels were detached using a single channel pipette (P200) by strongly pipetting buffer up and down in the 24-well plates. Lenses were transferred to cover glasses in dishes (35 × 10 mm). Images of hyaloid-retinal vessels were observed using fluorescence stereomicroscopy.

the diameter of hyaloid-retinal vessels increased concentration-dependently, from 30 to 135 mM glucose (Figure 2A). Furthermore, we observed that the proportion of lenses containing vessels with diameter more than 1.5 AU (artificial unit) also increased with the concentration of glucose, from about 20% of lenses with large vessels at 30mM glucose to just over 80% of lenses at 130mM (Figure 2B). This effect is referred to as inductivity. The effects of these conditions on the survival of the larvae is shown in Figure 2C. Survival was unaffected, compared with control (0 mM glucose) values, from 30 to 120 mM glucose. However, at 135 and 150 mM glucose there was a significant decrease in survival at 6 dpf.

On the basis of the results shown in Figure 2, we chose 130mM glucose as a standard treatment to induce changes in the retinal vessels and this is referred to as the HG condition. Under these HG conditions, we examined the vessel diameter, the rate of induction , overall survival rates and glucose levels in the zebrafish larvae, along with other aspects of embryonic development, as described below (Figure 3). In 10 preparations, HG treatment did not induce the dilated

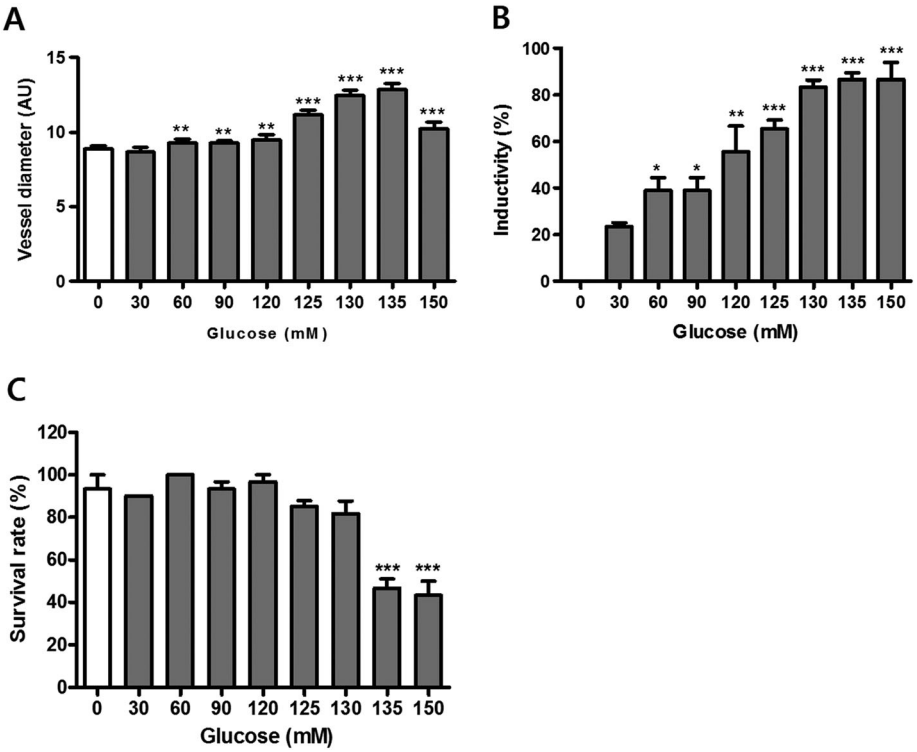

Figure 2

Effects of glucose in 6 dpf zebrafish larvae were concentration-dependent. Glucose 30–150 mM was added for 3 days (from 3 to 6 dpf). (A) The diameter of hyaloid-retinal vessels increased in a concentration-dependent manner. The graph displays the mean artificial unit for vessel diameter. The vessel diameter of each lens was measured three times. $^{**}P < 0.01$, $^{***}P < 0.001$, significantly different from control, $n = 8$–10 embryos per group. (B) Inductivity for vessel diameter increased in a dose-dependent manner. $^{*}P < 0.05$, $^{**}P < 0.01$, $^{***}P < 0.001$, significantly different from control, $n = 8$–10 embryos per group. (C) Survival rates after exposure to glucose (30-150mM) in developing zebrafish larvae at 6 dpf ($n = 10$). $^{***}P < 0.001$, significantly different from control.

retinal vessels in 3 samples (Figure 3A). This phenomenon is thought to be modulated by different individuals. In the 7 preparations that did show these changes, the inductivity was 75% (Figure 3B). Under the HG conditions, the overall survival rate was approximately 80% (Figure 3C). Apart from the changes in the hyaloid-retinal vessels, there were no obvious differences in the structural development of the embryos, as assessed by microscopic observation, between the HG group and the control group (Figure 3B, C and E). In addition, glucose levels in whole embryo lysates were measured and found to be much higher in the HG group than those in the control group (Figure 3D).

Because changes in the size of the retinal vessels could reflect changes in the size of the lens itself, we measured the lens size in the HG and control groups. As shown in Figure S2A, there was no significant difference in lens size between these two experimental groups. Moreover there was no difference in the number of OD branches in the HG and control groups (Figure S2B).

As the HG conditions affected the hyaloid-retinal vessels, we looked for changes in other parts of the vasculature, using confocal microscopy. With this method we were able to see through the lens to the hyaloid-retinal vessels in zebrafish larvae and were able to confirm that HG treatment increased the diameter, compared with control conditions (Figures S3A, 3B and 3C). However, the diameters of blood vessels in the body parts present from the ninth segment to the 14 segment and of the intersomitic vessels (ISVs) and the dorsal aorta (DA) showed no significant differences between the HG and control groups (Figures S3A and 3B).

Effects of mannitol and $CoCl_2$ on zebrafish hyaloid vessels. Next, we assessed the contribution of the osmotic pressure of the HG treatment (the glucose concentration is 130 mM) to the changes in the hyaloid-retinal vessels in zebrafish larvae, by using 130mM mannitol instead of glucose for the 3 days from 3-6dpf. As shown in Figure 4, the hyaloid-retinal vessels of mannitol-treated larvae were not affected compared with the control vessels, whereas the HG treatment clearly increased the vessel diameter.

Another physical change associated with DR is hypoxia (Geoffrey and Sobha, 2011) and hypoxic conditions have induced retinopathy in adult zebrafish (Cao *et al.*, 2010). We therefore evaluated the effects of hypoxia induced by $CoCl_2$ on the hyaloid-retinal vessels. In these experiments, we exposed the zebrafish embryos to 120 μM $CoCl_2$, instead of glucose, from 3-6dpf and found that this condition of hypoxia was as effective as HG in increasing the diameter of the hyaloid-retinal vessels (Figure 4A, B and D).

HG-induced vessel dilation leads to a defect in tight-junction proteins. In DR, pericyte loss and vessel thickening lead to compromised integrity of the vascular walls, resulting in increased permeability and changes in tight junction protein formation in retinal vessels (Bergers and Song, 2005;

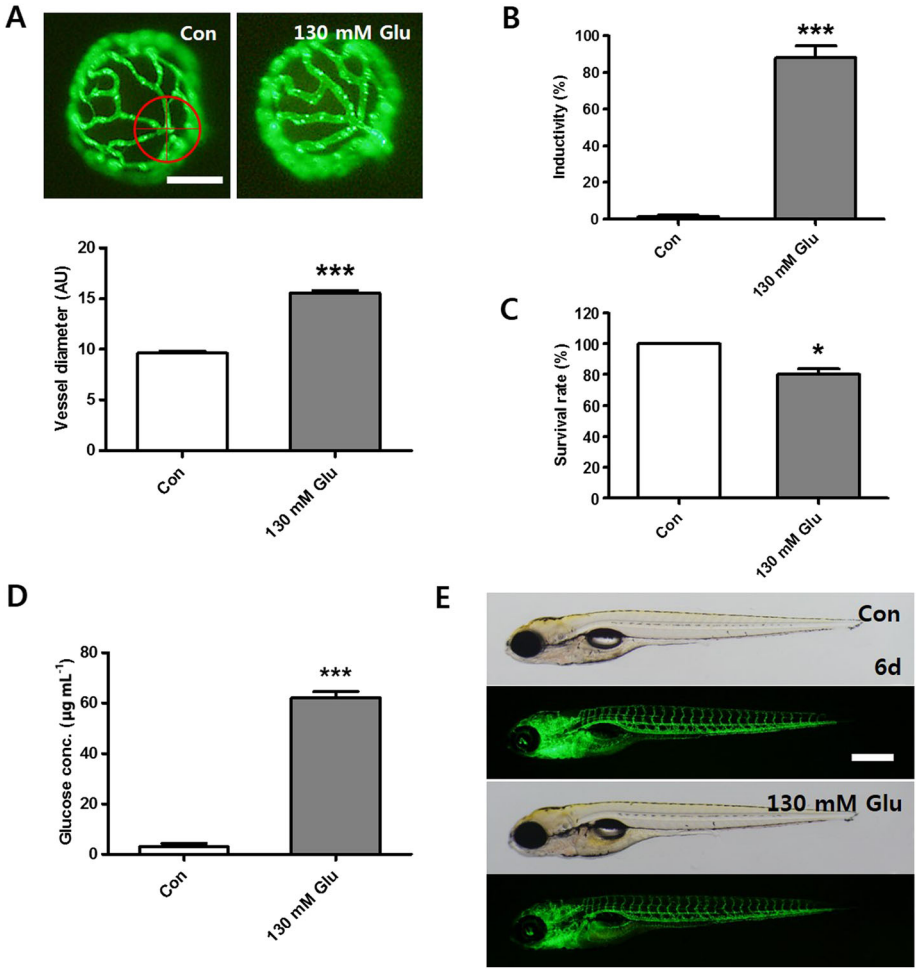

Figure 3

Changes in hyaloid-retinal vessel diameter induced by 130 mM glucose(HG). (A) The average diameter and fluorescent images of hyaloid-retinal vessels in HG-treated larvae. The diameter of hyaloid-retinal vessels was measured at locations proximal (red circle) to the OD from each group. The graph displays the mean AU for vessel diameter. The vessel diameter of each lens was measured three times. ***$P < 0.001$, significantly different from control, $n = 8$–10 embryos per group. Scale bar = 40 μm. (B) Inductivity for the vessel diameter was increased in the HG-treated group, compared with the control group. ***$P < 0.001$, significantly different from control, $n = 8$–10 embryos per group. (C) Survival rates in HG-treated zebrafish larvae. *$P < 0.05$, significantly different from control, $n = 10$ embryos per group. (D) After HG-treatment for 3 days, the zebrafish displayed increased levels of glucose. ***$P < 0.001$, significantly different from control, $n = 20$ embryos per group. (E) Control and HG-treated larvae did not show gross morphological changes at 6dpf. Scale bar = 300 μm.

Pfister *et al.*, 2008). As shown in Figure 5A and D, at 6 dpf, after 3 days of HG treatment, the overall diameter of hyaloid-retinal vessels in the HG-treated zebrafish larvae was thicker than that in the control vessels. The tight junction protein. ZO-1 is an intracellular adaptor protein that regulates permeability in the retinal vasculature. When we measured expression of this tight junction protein in hyaloid-retinal vessels, using a ZO-1-specific antibody, we found that expression of this protein in the vessels from from HG-treated larvae showed markedly irregular and discontinuous staining, compared with the staining in control vessels (Figure 5B and E).

Effects of VEGF signalling and the VEGFR inhibitor in HG-induced larvae

The mitogenic cytokine VEGF exhibits potent pro-angiogenic activity and also increases vascular permeability. Moreover, VEGF has been implicated in the pathogenesis of DR through angiogenesis induced by binding to VEGFR2 in endothelial cells (Sheetz and King, 2002; Caldwell *et al.*, 2003; Scheppke *et al.*, 2008). We therefore assessed the role of VEGF in our model of DR.

First, we examined the effects of inhibiting VEGF signalling using a VEGFR tyrosine kinase inhibitor (0.5 or 1 μM), added to the HG treatment, from 3 to 6 dpf, of zebrafish larvae. As shown in Figure 6A and 6B, the addition of the VEGF inhibitor blocked the effects of HG treatment on the vessels and, at the higher concentration (1 μM), treated vessels were identical to those in control larvae. Next, we wanted to evaluate the expression of the *Vegf*165 gene in hyaloid-retinal vessels. However, due to the small body size of zebrafish larvae, it is not possible to isolate specific tissues for tissue-specific mRNA quantifications without noticeable contamination from surrounding tissues. So we carried out our evaluation using RT-PCR and mRNAs extracted from whole

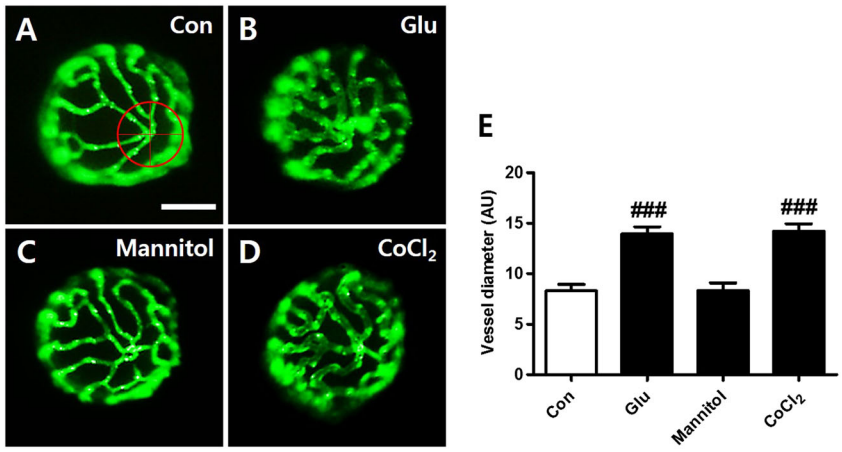

Figure 4

Effects of mannitol and $CoCl_2$ on hyaloid vessels of zebrafish larvae. [(A)–(D)] To assess possible effects of the hyperosmolarity of the HG treatment, mannitol (130 mM) was added instead of glucose. HG-treated larvae (B) showed dilated hyaloid vessels compared to the control (A), whereas hyaloid vessels of the mannitol-treated larvae (C) were not affected. (D) The effects of hypoxic conditions on hyaloid vessel development from 3-6 dpf was studied by adding $CoCl_2$ (120 μM) instead of glucose (130 mM) for three days. Under these conditions of hypoxia, we found dilated hyaloid vessels, similar to those after HG exposure (B). Scale bar = 40 μm. (E) Graph data are displayed as the mean AU for vessel diameter. The diameter of each lens was measured three times. ###$P < 0.001$, significantly different from control, n = 16–20 embryos per group.

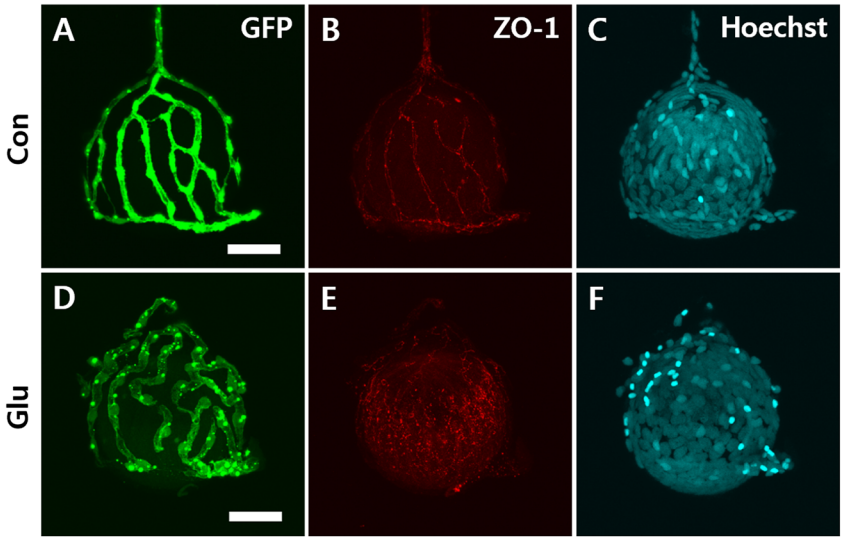

Figure 5

Expression of the tight junction protein ZO-1ion hyaloid-retinal vessels of HG-treated larvae. Confocal immunofluorescence microscopy images of hyaloid-retinal vessels on the dissected lens after treatment with trypsin. The overall morphology of hyaloid-retinal vessels was viewed with a confocal microscope in control and HG-treated larvae. Scale bar = 40 μm. Hyaloid-retinal vessels in HG-induced larvae were significantly thicker than control [(A) and (D)]. The expression of ZO-1 showed irregular and discontinuous staining on hyaloid-retinal vessels from HG-treated larvae (E) compared to control (B). To identify cells, Hoechst nuclear stain was used [(C) and (F)].

body lysates. As shown in Figure 6C and D, *Vegf*165 mRNA was up-regulated in larvae after HG-treatment from 3-6dpf, compared with control larvae and this increase was clearly prevented by addition of the VEGFR inhibitor.

To further validate our model, we used a monoclonal antibody to VEGF, ranibizumab (Lucentis), which has been used clinically for the treatment of retinal neovascularization. This antibody was added to the HG treatment for 3 days and substantially prevented the increase in vessel diameter induced by HG treatment alone (Figure 6E). The effects of the ranibizumab were significant only at the higher concentration used (2.5μg mL^{-1}; Figure 6F).

NO activation and the effect of L-NAME on the dilation of hyaloid-retinal vessels after HG-treatment

Signalling by NO is important for regulating blood vessel dilation and HG conditions are known to increase NOS expression (Francesco *et al.*, 1997). Zebrafish larvae produce NO, and this

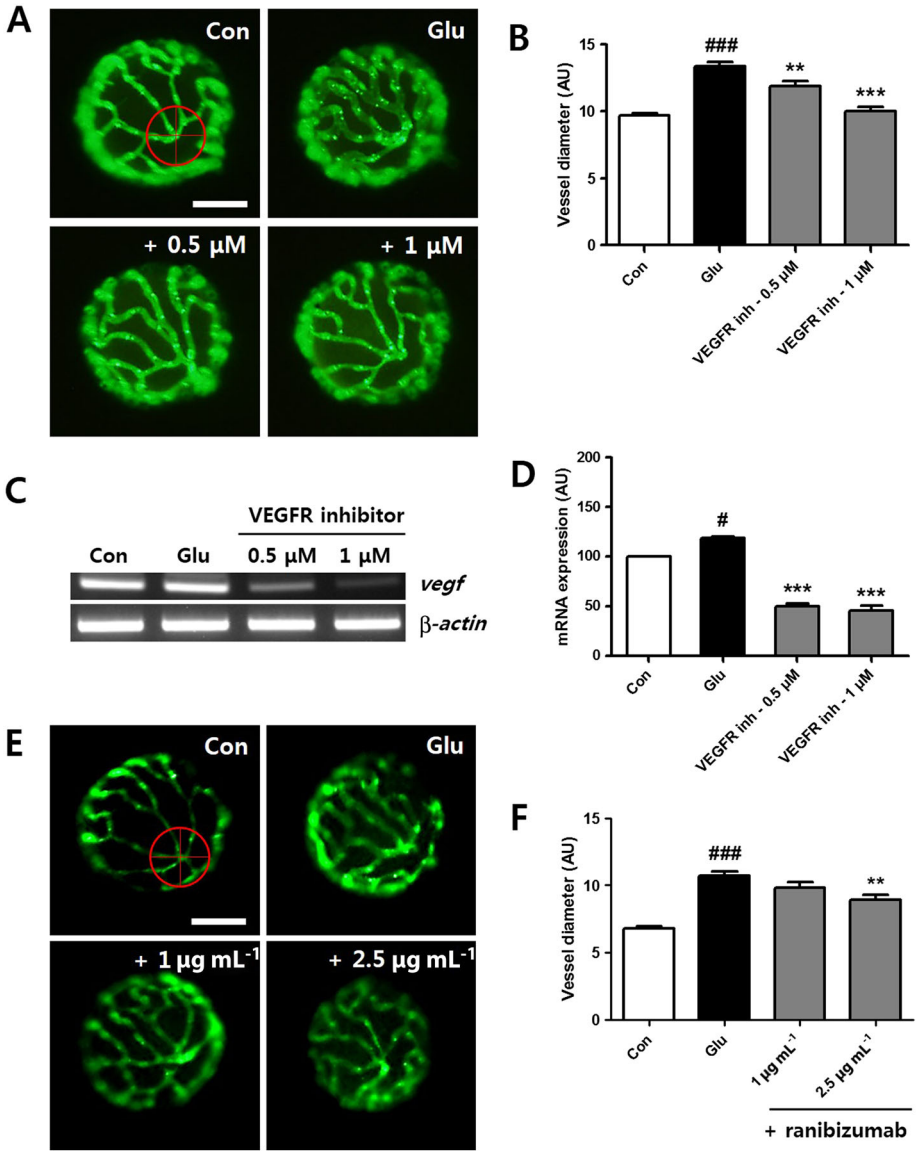

Figure 6

Vegf expression and the effect of the VEGFR inhibitor and the VEGF antibody ranibizumab in HG-treated larvae. (A) The effect of the VEGFR inhibitor on dilated hyaloid-retinal vessels. Vessel dilation induced by HG was blocked by treatment with the VEGFR tyrosin kinase inhibitor (0.5 or 1 μM). Scale bar = 40 μm. (B) The diameter of hyaloid-retinal vessels in HG-treated larvae with VEGFR inhibition was similar to control. Graph data are displayed as the mean AU for vessel diameter. ###$P < 0.001$ versus control; **$P < 0.01$, ***$P < 0.001$, significantly different from HG, n = 8–10 embryos per group. The vessel diameter of each lens was measured three times. [(C) and (D)] Expression of *Vegf* in HG-treated larvae increased significantly compared with control and was reduced by treatment with the VEGFR inhibitor. No changes in the transcript levels of β-*actin* were detected between control and HG-treated larvae. #$P < 0.05$, significantly different from control; ***$P < 0.001$, significantly different from HG. (E) The effect of the VEGF antibody, ranibizumab, on dilated hyaloid-retinal vessels. HG-induced vessel dilation was morphologically rescued by ranibizumab treatment (2.5 μg·mL^{-1}). Scale bar = 40 μm. (F) The diameter of hyaloid-retinal vessels in HG-treated larvae with ranibizumab treatment was significantly reduced. Graph data are displayed as the mean AU for vessel diameter. ###$P < 0.001$, significantly different from control; **$P < 0.01$, significantly different from HG, n = 8–10 embryos per group. The vessel diameter of each lens was measured three times.

signal can be live imaged in larvae incubated with a DAF-FM DA probe (Lepiller *et al.*, 2007). In our system, , we exposed the control and experimental groups of larvae at 6 dpf to DAF-FM DA and observed the results using confocal microscopy. We were able to identify NO production in the region of the notochord, cleithrum, and heart (data not shown). Interestingly, in hyaloid-retinal vessels, NO production was induced in HG-treated larvae but was not induced in control larvae (Figure 7A). Next, we used an NO inhibitor,,L-NAME, (10 or 20 μM) added to the HG treatment for 3 days and found that the hyaloid-retinal vessels from larvae treated with HG and L-NAME showed decreased vessel diameter, similar to the control group (Figure 7B and C). We also analysed the expression of mRNA for *nos2a* in the larvae. As shown in Figure 7D and E, mRNA expression of *nos2a* was increased, relative to control, in the larvae treated with HG and that this increase was significantly reduced by treatment with L-NAME.

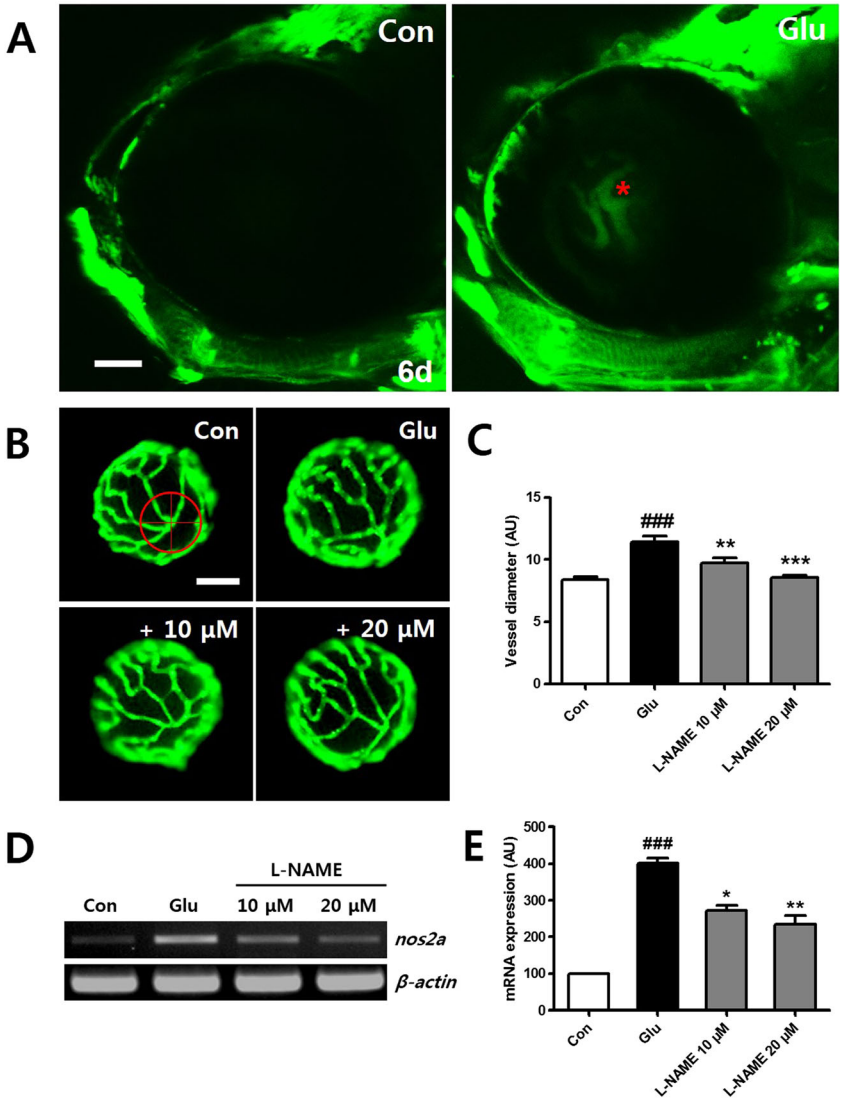

Figure 7

NO production by HG in hyaloid-retinal vessels. (A) Comparison of NO production using a DAF-FA DA probe in hyaloid-retinal vessels in control larvae at 6 dpf. NO production is not observed in control larvae but is detected in HG-treated larvae (red asterisk). Scale bar = 50 μm. (B) The effect of the NO inhibitor on dilated hyaloid-retinal vessels. HG-induced vessel dilation was rescued by the NOS inhibitor (L-NAME, 10 and 20 μM). (C) Graph data are displayed as the mean AU for vessel diameter. The vessel diameter of each lens was measured three times. Scale bar = 40 μm. ###$P < 0.001$ versus control; **$P < 0.01$, ***$P < 0.001$, significantly different from HG, $n = 10$ embryos per group. [(D) and (E)] Expression of *nos2a* in HG-treated larvae increased significantly compared to control and reduced by treatment with L-NAME. No changes in the transcript levels of β-*actin* were detected between control and HG-treated larvae. ###$P < 0.001$, significantly different from control; *$P < 0.05$, **$P < 0.01$, significantly different from HG.

Discussion and conclusions

During the last two decades, models of diabetes have been developed in many species, including pigs, dogs, cats, rats and mice, using different inducing agents such as chemicals (STZ or alloxan) or genetic modifications (Feit-Leichman *et al.*, 2005; Robinson *et al.*, 2012). Studies of the molecular pathways involved in DR have used STZ- or alloxan-induced diabetes models or transgenic and knockout mouse models such as *ob*/*ob* and *db*/*db* (Midena *et al.*, 1989; Cheung *et al.*, 2005; Zhang *et al.*, 2007). The retinae of STZ-induced diabetic animals exhibit biochemical and physiological changes 1–2 months after the onset of hyperglycaemia. This model reproduces early symptoms of DR, such as thickening of the vascular basement membrane, loss of retinal pericytes and capillaries, vascular occlusion and increased vascular permeability (Robinson *et al.*, 2012). A recent study suggested an animal model for non-proliferative DR in adult zebrafish, in which the zebrafish are subjected to 2% glucose (110 mM) immersion for 30 days (Alvarez *et al.*, 2010). In this model, visual function is diminished, and cone photoreceptors are disrupted. Hypoxia-induced retinal vascular disorder in the adult zebrafish model takes 11 days to show retinopathy and, consequently, to assess therapeutic effects (Cao *et al.*, 2010). In addition, these adult zebrafish models require testing several drug compounds in the plastic containers, and isolation of the retina vessels is time-consuming, requiring surgical microscissors and forceps resulting in physical stress.

Recently, Wang *et al.* (2013) reported that combination of a high cholesterol diet and immersion in a 3% glucose (166 mM) solution applied to 5 to 15 dpf zebrafish larvae could be used as a model for diabetic vasculopathy. Earlier studies showed that 1 dpf zebrafish larvae could be exposed to 30 mM glucose and drugs for to 6 days (Lee *et al.*, 2013; Yu *et al.*, 2013). In the present study, we have attempted to optimize and characterize a short-term in zebrafish to study diabetic retinal vascular dysfunction and provide a system for rapid drug screening. We induced hyperglycaemia by immersing 3 dpf zebrafish larvae for 3 days in 130 mM glucose (HG; Figures 2 and 3). Although there were clear changes in the hyaloid-retinal vessels, the lens size and number of OD branches were not affected. (Figure S2). Moreover, other bloods vessels such as ISVs and DA. did not show any differences between the control and HG groups (Figure S3).

In the present model, the hyaloid-retinal vessels were analysed after only 3 days incubation in 24-well plates. This procedure provides two advantages, a low incubation volume means that less drug is needed per test and the 3 days is clearly much shorter than 11 (Cao *et al.*, 2010) or 30 days (Alvarez *et al.*, 2010), as used previously. The structural changes in the hyaloid-retinal vessels after HG were not osmotic events but were influenced by *in vivo* glucose metabolism in zebrafish larvae. Gleeson *et al.* (2007) and Wang *et al.* (2013) reported that larvae treated with HG regulate glucose metabolism through direct secretion of insulin, phosphoenolpyruvate carboxykinase, somatostatin and glucagon into the bloodstream. These results suggest that HG-induced changes in zebrafish larvae hyaloid-retinal vessels closely mimic the molecular mechanism for human DR.

Reduction and redistribution of tight junction proteins in retinal endothelial cells under hyperglycaemic conditions increases vascular permeability (Antonetti *et al.*, 1998). Kim *et al.* (2011) did not observe occludin and ZO-1 expression on retinal vessels when viewed on whole mounts of frozen sections with immunofluorescence staining in zebrafish. However, using our isolation method and quantitative analyses (Figure 1 and S1), we were able to demonstrate expression of the tight junction protein ZO-1 and show that its expression was irregular or discontinuous on hyaloid-retinal vessels from HG-treated larvae (Figure 5).

At present, VEGF constitutes an exciting target for therapeutic intervention in DR. VEGF-induced angiogenesis and vascular hyperpermeability are mediated by NO (Van der Zee *et al.*, 1997). Also NO was an essential downstream component of VEGF-induced angiogenesis *in vivo* and NOS inhibitors blocked the VEGF-induced proliferation of endothelial cells (Shizukuda *et al.,* 1999). In the present experiments, we have confirmed that this model was sensitive to VEGF-related and NO-related interventions. Although early (0–1 dpf) exposure to a VEGFR inhibitor induced severe developmental defects, including heart and eye oedema, short body and developmental retardation (data not shown), later application, at 3 to 6 dpf, blocked the increase in diameter of retinal vessels, induced by HG treatment (Figure 6A and B).

As 75% of the protein sequence in zebrafish VEGFAA is similar to that of human VEGF-A 165 isoform (Wu *et al.*, 2015) and the recombinant humanized monoclonal IgG antibody for VEGF, ranibizumab, has been used to treat human DR by blocking angiogenesis, it was reasonable to test ranibizumab in our model. We also assessed NO production with a fluorescent indicator dye (DAF-FA DA) and the expression of NOS mRNA, in our model. These results and those after application of the NOS inhibitor L-NAME together demonstrated clearly that NO was an important mediator of the structural changes in the hyaloid-retinal vessels of zebrafish larvae following HG treatment. Overall, our results suggest that NO and VEGF in HG-treated zebrafish larvae display regulatory patterns and activities, very similar to those in mammals

Although several animal models for DR are well established, there are no short-term *in vivo* models to test the effects of candidate therapeutic compounds. In this study, we have described a novel, short-term, *in vivo* screening method for compounds affecting DR, using zebrafish larvae exposed to HG conditions. In this model, dilation of hyaloid-retinal vessels was accompanied by morphological lesions with disruption of tight junction proteins, overproduction of *Vegf* mRNA and NO production. We also showed that the VEGFR tyrosine kinase inhibitor, the VEGF antibody ranibizumab and inhibition of endogenous NO synthesis could all decrease or reverse the HG-induced dilation of hyaloid-retinal vessels. These results suggest that this zebrafish model system will be a powerful novel tool for the screening of therapeutic drug candidates for DR.

Acknowledgement

This research was supported by grants (K14040 and K15270) from the Korea Institute of Oriental Medicine (KIOM).

Author contributions

S-H.J, Y. S.K and J. S.K designed the experiments. S-H.J and Y-R.L performed the experiments and contributed to the zebrafish experiments. S-H.J, Y. S.K and Y-R.L analysed the data. S-H.J, Y. S.K and J. S.K wrote the manuscript. J. S.K. supervised the work. All authors provided comments on initial and final drafts of the manuscript.

Conflict of interest

The authors declare they have no conflict of interest.

References

Alexander SPH, Benson HE, Faccenda E, Pawson AJ, Sharman JL, Spedding M *et al.* (2013a). The Concise Guide to PHARMACOLOGY 2013/14: Catalytic Receptors. Br J Pharmacol 170: 1676–1705.

Alexander SPH, Benson HE, Faccenda E, Pawson AJ, Sharman JL, Spedding M *et al.* (2013b). The Concise Guide to PHARMACOLOGY 2013/14: Enzymes. Br J Pharmacol 170: 1797–1867.

Alvarez Y, Cederlund ML, Cottell DC, Bill BR, Ekker SC, Torres-Vazquez J *et al.* (2007). Genetic determinants of hyaloid and retinal vasculature in zebrafish. BMC Dev Biol 7: 114–130.

Alvarez Y, Chen K, Reynolds AL, Waghorne N, O'Connor JJ, Kennedy BN (2010). Predominant cone photoreceptor dysfunction in a hyperglycaemic model of non-proliferative diabetic retinopathy. Dis Model Mech 3: 236–245.

Abu El-Asrar AM, Meersschaert A, Dralands L, Geboes K (2004). Inducible nitric oxide synthase and vascular endothelial growth factor are colocalized in the retinas of human subjects with diabetes. Eye 18: 306–313.

Antonetti DA, Barber AJ, Khin S, Lieth E, Tarbell JM, Gardner TW (1998). Vascular permeability in experimental diabetes is associated with reduced endothelial occludin content: vascular endothelial growth factor decreases occludin in retinal endothelial cells. Penn State Retina Res Group Diab 47: 1953–1959.

Armulik A, Abramsson A, Betsholtz C (2005). Endothelial/pericyte interactions. Circ Res 97: 512–523.

Barros TP, Alderton WK, Reynolds HM, Roach AG, Berghmans S (2008). Zebrafish: an emerging technology for in vivo pharmacological assessment to identify potential safety liabilities in early drug discovery. Br J Pharmacol 154: 1400–1413.

Bergers G, Song S (2005). The role of pericytes in blood-vessel formation and maintenance. Neuro Oncol 7: 452–464.

Calcutt NA, Cooper ME, Kern TS, Schmidt AM (2009). Therapies for hyperglycaemia-induced diabetic complications: from animal models to clinical trials. Nat Rev Drug Discov 8: 417–429.

Caldwell RB, Bartoli M, Behzadian MA, EI-Remessy AE, AI-Shabrawey M, Platt DH *et al.* (2003). Vascular endothelial growth factor and diabetic retinopathy: pathophysiological mechanisms and treatment perspectives. Diabetes Metab Res Rev 19: 442–455.

Cao Z, Jensen LD, Rouhi P, Hosaka K, Lanne T, Steffensen JF *et al.* (2010). Hypoxia-induced retinopathy model in adult zebrafish. Nat Protoc 5: 1903–1910.

Checchin D, Sennlaub F, Levavasseur E, Leduc M, Chemtob S (2006). Potential role of microglia in retinal blood vessel formation. Invest Ophthalmol Vis Sci 47: 3595–3602.

Cheung AK, Fung MK, Lo AC, Lam TT, So KF, Chung SS *et al.* (2005). Aldose reductase deficiency prevents diabetes-induced blood-retinal barrier breakdown, apoptosis, and glial reactivation in the retina of db/db mice. Diabetes 54: 3119–3125.

Elo B, Villano CM, Govorko D, White LA (2007). Larval zebrafish as a model for glucose metabolism: expression of phosphoenolpyruvate carboxykinase as a marker for exposure to anti-diabetic compounds. J Mol Endocrinol 38: 433–440.

Engerman RL, Kern TS (1995). Retinopathy in animal models of diabetes. Diabetes Metab Rev 11: 109–120.

Feit-Leichman RA, Kinouchi R, Takeda M, Fan Z, Mohr S, Kern TS *et al.* (2005). Vascular damage in a mouse model of diabetic retinopathy: relation to neuronal and glial changes. Invest Ophthalmol Vis Sci 46: 4281–4287.

Fong DS, Aiello L, Gardner TW, King GL, Blankenship G, Cavallerano JD *et al.* (2003). Diabetic retinopathy. Diabetes Care 26: 226–229.

Francesco C, Keiichi H, Zvonimir SK, Thomas FL (1997). High glucose increases nitric oxide synthase expression and superoxide anion generation in human aortic endothelial cells. Circulation 96: 25–28.

Geoffrey BA, Sobha S (2011). Hypoxia and oxidative stress in the causation of diabetic retinopathy. Curr Diabetes Rev 7: 291–304.

Gleeson M, Connaughton V, Arneson LS (2007). Induction of hyperglycaemia in zebrafish (Danio rerio) leads to morphological changes in the retina. Acta Diabetol 44: 157–163.

Greene DA, Arezzo JC, Brown MB (1999). Effect of aldose reductase inhibition on nerve conduction and morphometry in diabetic neuropathy. Zenarestat Study Group. Neurology 53: 580–591.

Guillemin GJ, Brew BJ (2004). Microglia, macrophages, perivascular macrophages, and pericytes: a review of function and identification. J Leukoc Biol 75: 388–397.

Jorgens K, Hillebrands JL, Hammes HP, Kroll J (2012). Zebrafish: a model for understanding diabetic complications. Exp Clin Endocrinol Diabetes 120: 186–187.

Joussen AM, Poulaki V, Qin W, Kirchhof B, Mitsiades N, Wiegand SJ *et al.* (2002). Retinal vascular endothelial growth factor induces intercellular adhesion molecule-1 and endothelial nitric oxide synthase expression and initiates early diabetic retinal leukocyte adhesion in vivo. Am J Pathol 2: 501–509.

Jung SH, Kim S, Chung AY, Kim HT, So JH, Ryu J *et al.* (2010). Visualization of myelination in GFP-transgenic zebrafish. Dev Dyn 2: 592–597.

Kempen JH, O'Colmain BJ, Leske MC, Haffner SM, Klein R, Moss SE *et al.* (2004). The prevalence of diabetic retinopathy among adults in the United States. Arch Ophthalmol 122: 552–563.

Kilkenny C, Browne WJ, Cuthill IC, Emerson M, Altman DG (2010). Animal research: Reporting in vivo experiments: The ARRIVE guidlines. Br J Pharmacol 160: 1577–1579.

Kim JH, Yu YS, Kim KW, Kim JH (2011). Investigation of barrier characteristics in the hyaloid-retinal vessel of zebrafish. J Neurosci Res 89: 921–928.

Kitambi SS, McCulloch KJ, Peterson RT, Malicki JJ (2009). Small molecule screen for compounds that affect vascular development in the zebrafish retina. Mech Dev 126: 464–477.

Lakshminarayanan S, Antonetti DA, Gardner TW, Tarbell JM (2000). Effect of VEGF on retinal microvascular endothelial hydraulic conductivity: the role of NO. Invest Ophthalmol Vis Sci 41: 4256–4261.

Lee IS, Yu SY, Jung SH, Lee YR, Lee YM, Kim JH *et al.* (2013). Proanthocyanidins from *Spenceria ramalana* and their effects on AGE formation in vitro and hyaloid-retinal vessel dilation in larval zebrafish in vivo. J Nat Prod 76: 1881–1888.

Lepiller S, Laurens V, Bouchot A, Herbomel P, Solary E, Chluba J (2007). Imaging of nitric oxide in a living vertebrate using a diamino-fluorescein probe. Free Radic Biol Med 43: 619–627.

Liang J, Gui Y, Wang W, Gao S, Li J, Song H (2010). Elevated glucose induces congenital heart defects by altering the expression of tbx5, tbx20, and has2 in developing zebrafish embryos. Birth Defects Res A Clin Mol Teratol 88: 480–486.

McGrath JC, Drummond GB, McLachlan EM, KilKenny C, Wainwright CL (2010). Guidelins for reporteing experiments involving animals: the ARRIVE guidlines. Br J Pharmacol 160: 1573–1576.

Midena E, Segato T, Radin S, di Giorgio G, Meneghini F, Piermarocchi S *et al.* (1989). Studies on the retina of the diabetic db/db mouse. I. Endothelial cell-pericyte ratio. Ophthalmic Res 21: 106–111.

Morbidelli L, Chang CH, Douglas JG, Granger HJ, Ledda F, Ziche M (1996). Nitric oxide mediates mitogenic effect of VEGF on coronary vascular endothelium. Am J Physiol 270: H411–415.

Nusslein VC, Dahm R (eds) (2002). Zebrafish: A Practical Approach. Oxford University Press: Oxford, UK.

Pawson AJ, Sharman JL, Benson HE, Faccenda E, Alexander SP, Buneman OP *et al.* (2014). The IUPHAR/BPS Guide to PHARMACOLOGY: an expert-driven knowledge base of drug targets and their ligands. Nucl Acids Res 42 (Database Issue): D1098–1106.

Pfister F, Feng Y, vom Hagen F, Hoffmann S, Molema G, Hillebrands JL *et al.* (2008). Pericyte migration: a novel mechanism of pericyte loss in experimental diabetic retinopathy. Diabetes 57: 2495–2502.

Robinson R, Barathi VA, Chaurasia SS, Wong TY, Kern TS (2012). Update on animal models of diabetic retinopathy: from molecular approaches to mice and higher mammals. Dis Model Mech 5: 444–456.

Roy MS, Klein R, O'Colmain BJ, Klein BE, Moss SE, Kempen JH (2004). The prevalence of diabetic retinopathy among adult type 1 diabetic persons in the United States. Arch Ophthalmol 122: 546–551.

Scheppke L, Aguilar E, Gariano RF, Jacobson R, Hood J, Doukas J *et al.* (2008). Retinal vascular permeability suppression by topical application of a novel VEGFR2/Src kinase inhibitor in mice and rabbits. J Clin Invest 118: 2337–2346.

Sheetz MJ, King GL (2002). Molecular understanding of hyperglycemia's adverse effects for diabetic complications. JAMA 288: 2579–2588.

Shizukuda Y, Tang S, Yokota R, Ware JA (1999). Vascular endothelial growth factor-induced endothelial cell migration and proliferation depend on a nitric oxide-mediated decrease in protein kinase C_{δ} activity. Circ Res 85: 247–256.

Starita C, Patel M, Katz B, Adamis AP (2007). Vascular endothelial growth factor and the potential therapeutic use of pegaptanib (macugen) in diabetic retinopathy. Dev Ophthalmol 39: 122–148.

Van der Zee R, Murohara T, Luo Z, Zollmann F, Passeri J, LeKutat C *et al.* (1997). Vascular endothelial growth factor/vascular permeability factor augments nitric oxide release from quiescent rabbit and human vascular endothelium. Circulation 95: 1030–1037.

Wang Z, Mao Y, Cui T, Tang D, Wang XL (2013). Impact of a combined high cholesterol diet and high glucose environment on vasculature. PLoS One 12: e81485.

Wu YC, Chang CY, Kao A, Hsi B, Lee SH, Chen YH *et al.* (2015). Hypoxia-induced retinal neovascularization in zebrafish embryos: a potential model of retinopathy of prematurity. PLoS One 15: e0126750.

Yu SY, Lee IS, Jung SH, Lee YM, Lee YR, Kim JH *et al.* (2013). Caffeoylated phenylpropanoid glycosides from *Brandisia hancei* inhibit advanced glycation end product formation and aldose reductase in vitro and vessel dilation in larval zebrafish in vivo. Planta Med 79: 1705–1709.

Zhang H, Sonoda KH, Qiao H, Oshima T, Hisatomi T, Ishibashi T (2007). Development of a new mouse model of branch retinal vein occlusion and retinal neovascularization. Jpn J Ophthalmol 51: 251–257.

Supporting Information

Additional Supporting Information may be found in the online version of this article at the publisher's web-site:

http://dx.doi.org/10.1111/bph.13279

Figure S1 Diagram depicting measurement of the hyaloid-retinal vessels diameter. (A) Lens in a dish with a coverglass. (B) Lens alignments under the fluorescence microscope. The optic disc (OD) was displayed up. (C) Fluorescence microscopy images. (D) The diameter of hyaloid vessels was measured in three main branches (red arrow) from the OD into the first branch (~30 μm) using Image J software.

Figure S2 Morphological effects on the patterning of the hyaloid vessels and lens size by HG. (A) The size of lenses were normal in control and HG-treated larvae. Control larvae, n=38; HG-treated larvae, n=40. Scale bar = 40 μm. (B) The number of main branches from the optic disc (OD) was counted in control and glucose-treated larvae. Control larvae, n=76; HGtreated larvae, n=72. Scale bar = 40 μm.

Figure S3 Repersentative images of hyaloid-retinal vessels and trunk vessels in 6 dpf zebrafish. (A,A`,B,B`) There were no differences in intersomite vessels (ISVs) and dorsal aorta (DA) between the control (A, A`) and HG-treated groups (B, B`). 250´ magnification, n=4 in each group. Scale bar = 50 μm. (C-E) The graph displays the mean artificial unit (AU) for diameter of ISVs and DA. The vessel diameter of each region was measured three times. The experiment was repeated triplicate. *$P < 0.05$ vs. control.